Interannual Variability and Trends of Extratropical Ozone. Part II: Southern Hemisphere

XUN JIANG,*,+ STEVEN PAWSON,# CHARLES D. CAMP,@ J. ERIC NIELSEN,#,& RUN-LIE SHIA,* TING LIAO,** VARAVUT LIMPASUVAN++, AND YUK L. YUNG*

* *Division of Geological and Planetary Sciences, California Institute of Technology, Pasadena, California*
# *Global Modeling and Assimilation Office, NASA GSFC, Greenbelt, Maryland*
@ *Mathematics Department, California Polytechnic State University, San Luis Obispo, California*
& *Science Systems and Applications, Inc., Lanham, Maryland*
** *Department of Physics, California Institute of Technology, Pasadena, California*
++ *Department of Chemistry and Physics, Coastal Carolina University, Conway, South Carolina*

(Manuscript received 20 March 2008, in final form 1 April 2008)

ABSTRACT

A principal component analysis (PCA) is applied to the Southern Hemisphere (SH) total column ozone following the method established for analyzing the data in the Northern Hemisphere (NH) in a companion paper. The interannual variability (IAV) of extratropical O_3 in the SH is characterized by four main modes, which account for 75% of the total variance. The first two leading modes are approximately zonally symmetric and relate to the Southern Hemisphere annular mode and the quasi-biennial oscillation. The third and fourth modes exhibit wavenumber-1 structures. Contrary to the Northern Hemisphere, the third and fourth modes are not related to stationary waves. Similar results are obtained for the 30–100-hPa geopotential thickness. The decreasing O_3 trend in the SH is captured in the first mode. The largest trend is at the South Pole, with value ~ -2 Dobson Units (DU) yr^{-1}. Both the spatial pattern and trends in the column ozone are captured by the Goddard Earth Observation System chemistry–climate model (GEOS-CCM) in the SH.

1. Introduction

Dynamics can strongly modulate the interannual variability (IAV) of stratospheric ozone (Fusco and Salby 1999; Hood and Soukharev 2003; Randel et al. 2002). In the tropics, 93% of total column ozone interannual variability could be explained by four modes whose structures are attributable to the quasi-biennial oscillation (QBO), the interaction between the QBO and the annual beat (QBO-AB), the El Niño–Southern Oscillation (ENSO), and the solar cycle (Camp et al. 2003). A primary motivation for studying the IAV of column ozone is to separate the observed trends from the natural variability, especially in high latitudes. However, the principal IAV modes of stratospheric ozone and their relationship to IAV of dynamical influences are not known at high latitudes. This new knowledge can offer clues to improve our understanding of ozone variability and its connection to (and interaction with) climate changes. The extension of principal component analysis (PCA; Preisendorfer 1988) to the high latitudes was hampered by the fact that the most comprehensive merged ozone data (MOD) set (McPeters et al. 1996) lacks O_3 data in the polar night region.

In this paper, we apply PCA to the Southern Hemisphere (SH) total column ozone. A companion paper (Jiang et al. 2008, hereafter Part I) discusses a similar analysis for the Northern Hemisphere (NH). The SH has weaker planetary waves and therefore weaker Brewer–Dobson circulation and larger ozone trend. Therefore, the effects of ozone changes to the climate and dynamics in the SH are likely much larger than those in the NH. On the other hand, the change of dynamics would also affect the ozone, especially in the polar region. A new generation of coupled models is

+ Current affiliation: Department of Earth and Atmospheric Sciences, University of Houston, Houston, Texas.

Corresponding author address: Yuk L. Yung, Division of Geological and Planetary Sciences, California Institute of Technology, 1200 East California Boulevard, Pasadena, CA 91125.
E-mail: yly@gps.caltech.edu

DOI: 10.1175/2008JAS2793.1

being developed to simulate the interaction among ozone, greenhouse gases, and dynamics to predict the ozone recovery and climate change (e.g., Li et al. 2008; Shindell et al. 2006). A detailed analysis of ozone distribution using observed data would help to provide understand and improve the simulations of these models.

The data we used are based on a combination of the merged ozone dataset (McPeters et al. 1996) and the assimilated data from the European Centre for Medium-Range Weather Forecasts (ECMWF; Dethof and Holm 2004; Uppala et al. 2005). The ECMWF O_3 data are assimilated from January 1979 to December 1988 and from January 1991 to August 2002. Data are available on a 2.5° × 2.5° latitude–longitude grid. The details for the datasets are described in section 2. The results of PCA for the SH column ozone and geopotential thickness (GPT) are discussed in section 3. The IAV and trends of model O_3 in the SH are discussed in section 4. Extended discussions of how our principal findings, including those from Part I, relate to other studies are presented in section 5. Section 6 contains our conclusions and final remarks. In the appendix, we provide information on the validation of O_3 data, cylindrical projections, zonal mean, and *t* statistics of the leading modes in the SH. The presented results provide a complementary counterpart to the findings in the Northern Hemisphere of Part I, published in this same issue. Comparisons to the NH results of that study will be referred to throughout this paper.

2. Datasets

In this paper, we have used the same four datasets as those in Jiang et al. (2008). All data are the monthly mean data. The O_3 data are from the merged ozone dataset (McPeters et al. 1996), which has been extended to the poles using assimilated O_3 and potential vorticity (PV) from the 40-yr European Centre for Medium-Range Weather Forecasts (ECMWF) Re-Analysis (ERA-40) project (Dethof and Holm 2004; Simmons et al. 1999; Uppala et al. 2005). The MOD and ERA-40 ozone data are very similar where they overlap. The ECMWF O_3 has good agreement with the ozonesonde in the polar region after 1979, except that the ECMWF O_3 at the South Pole is slightly high in October (Dethof and Holm 2004). During 1989 and 1990 when the ECMWF assimilated O_3 were not available, ECMWF PV was used as a proxy for O_3 based on a mapping method (Manney et al. 1999). (Details of validating the ECMWF assimilated O_3 and ozonesonde are shown in Fig. A1 in the appendix.) To relate O_3 to atmospheric dynamics, we also investigate the 30–100-hPa geopotential thickness from the National Centers for Environmental Prediction (NCEP)–Department of Energy (DOE) Reanalysis 2 (hereafter, NCEP2) (Kalnay et al. 1996; Kistler et al. 2001). We also compare the column O_3 results from the Goddard Earth Observation System chemistry–climate model (GEOS-CCM; Stolarski et al. 2006a; Pawson et al. 2008). The GEOS-CCM is based on the GEOS-4 general circulation model (da Silva et al. 2005) and includes a stratospheric chemistry code (Stolarski et al. 2006b).

3. PCA of Southern Hemispheric column O_3 and GPT

a. Results for Southern Hemispheric column O_3

As shown in Fig. 1, the first four modes account for 43.9%, 13.7%, 9.8%, and 7.4% of the variance, together explaining over 74.8% of the O_3 variance in the SH (see Table 1). The first mode is zonally symmetric and strongly resembles the first mode in the NH. As expected, it is associated with the Southern Hemisphere annular mode (SAM; Limpasuvan and Hartmann 1999; Thompson and Wallace 2000). The second mode in the SH (Fig. 1b) has some resemblance to its NH counterpart in that it describes a see-saw pattern between the high and middle latitudes, changing sign at approximately 60°S. However, the meridional gradients at the vortex edge are weaker in the SH, where the high-latitude maximum is displaced from the pole. The last two modes are zonally asymmetric and they represent a wavenumber-1 structure as in the NH.

Figure 2a shows the first principal component (PC1; solid line) in the SH. For comparison, we also show the inverted SAM index (dotted line). The correlation between the detrended PC1 and detrended inverted SAM index is 0.45 (significant at the 0.1% level). A stronger polar vortex in the SH (positive SAM index) will lead to less ozone (negative PC1) in the high SH latitudes due to a weaker Brewer–Dobson circulation. In addition, a stronger Antarctic vortex with colder temperature will also lead to more chemical ozone loss. The power spectrum (Fig. 2b) of the detrended PC1 reveals 5% significant peaks at the residual annual cycle (A), 20 months (Q_1) (Tung and Yang 1994a,b; Jiang et al. 2005), and 6 months (A_1) (Gray and Pyle 1986). The trend of PC1 is much larger than that of SAM. This disparity suggests that the negative ozone trend in the SH cannot be accounted for by dynamics. Instead, the trend is mostly due to chemical loss. This is consistent with the concept that ozone isolated in the polar vortex responds to increases in stratospheric chlorine loading in later years, but that the fundamental nature of the Antarctic polar vortex has not changed. There is no

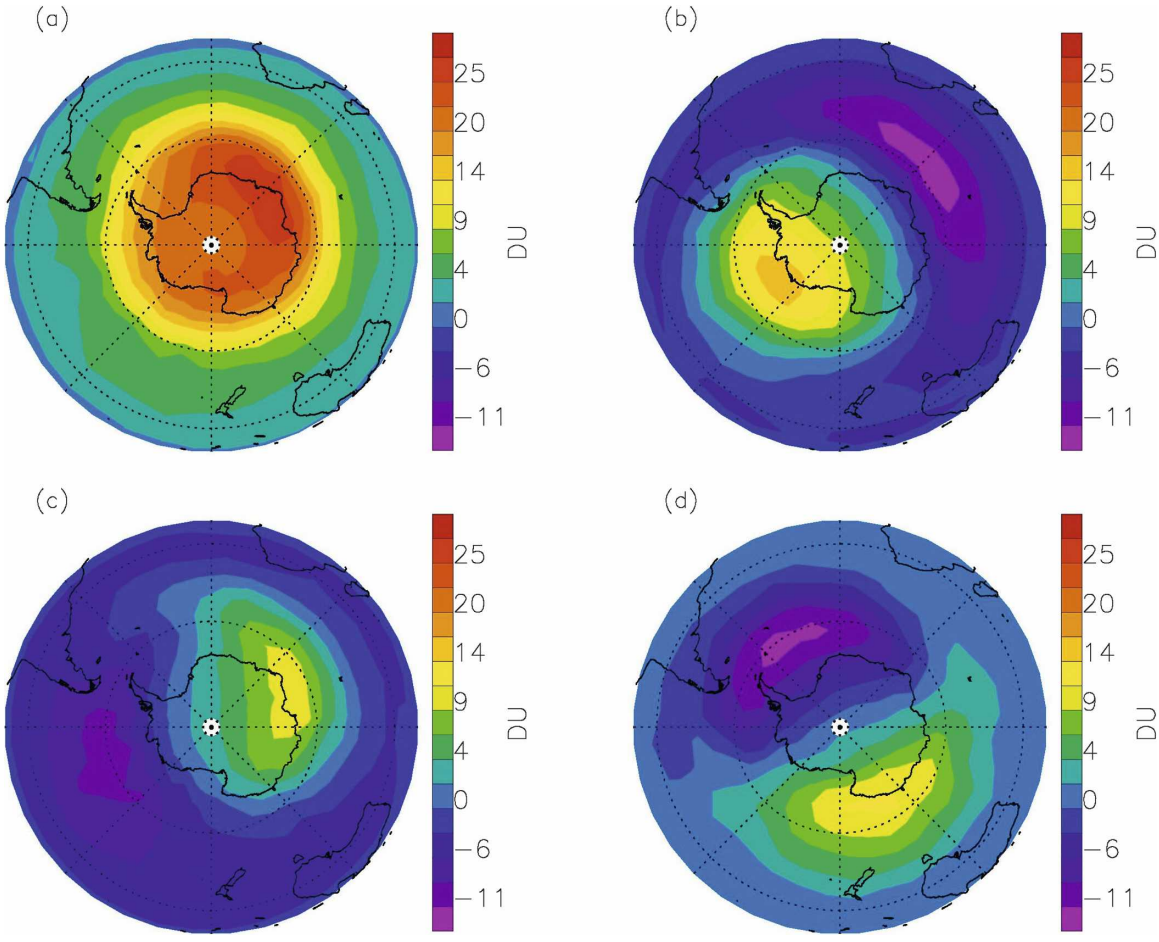

FIG. 1. The spatial patterns of the O_3 anomalies regressed upon the leading PCs in the SH. Units are DU. The first four modes explain 43.9%, 13.7%, 9.8%, and 7.4% of the total variance, respectively.

obvious volcanic impact on PC1 in the SH. The El Chichón aerosols remained mostly north of the equator, so there was less ozone depletion in the SH (Pollack et al. 1983; Zerefos et al. 1994). Although considerable amount of Pinatubo aerosols moved to the SH midlatitude (Trepte et al. 1993), the ozone depletion signal is very small (Zerefos et al. 1994; Coffey 1996) and may be embedded in the large natural variability. The spectral estimate of the detrended PC2 reveals significant peaks at the residual annual cycle (A) and at

TABLE 1. Comparison of the leading modes of variability in column O_3 and GPT in the SH.

Modes	1	2	3	4	Sum
Fractions of variance					
O3 in the SH	43.9%	13.7%	9.8%	7.4%	74.8%
GPT in the SH	29%	22.4%	18.9%	10.3%	80.6%
Spatial pattern					
O3 in the SH	Symmetric	Symmetric (off pole)	Wave 1	Wave 1	—
GPT in the SH	Symmetric (off pole)	Symmetric (off pole)	Wave 1	Wave 1	—
Temporal pattern					
O3 in the SH	SAM + trend QBO-AB, SAO	QBO, QBO-AB	Stochastic, QBO, QBO-AB	Stochastic, BO	—
GPT in the SH	SAM + trend QBO-AB, 8 months	8 yr	Stochastic	Stochastic	—

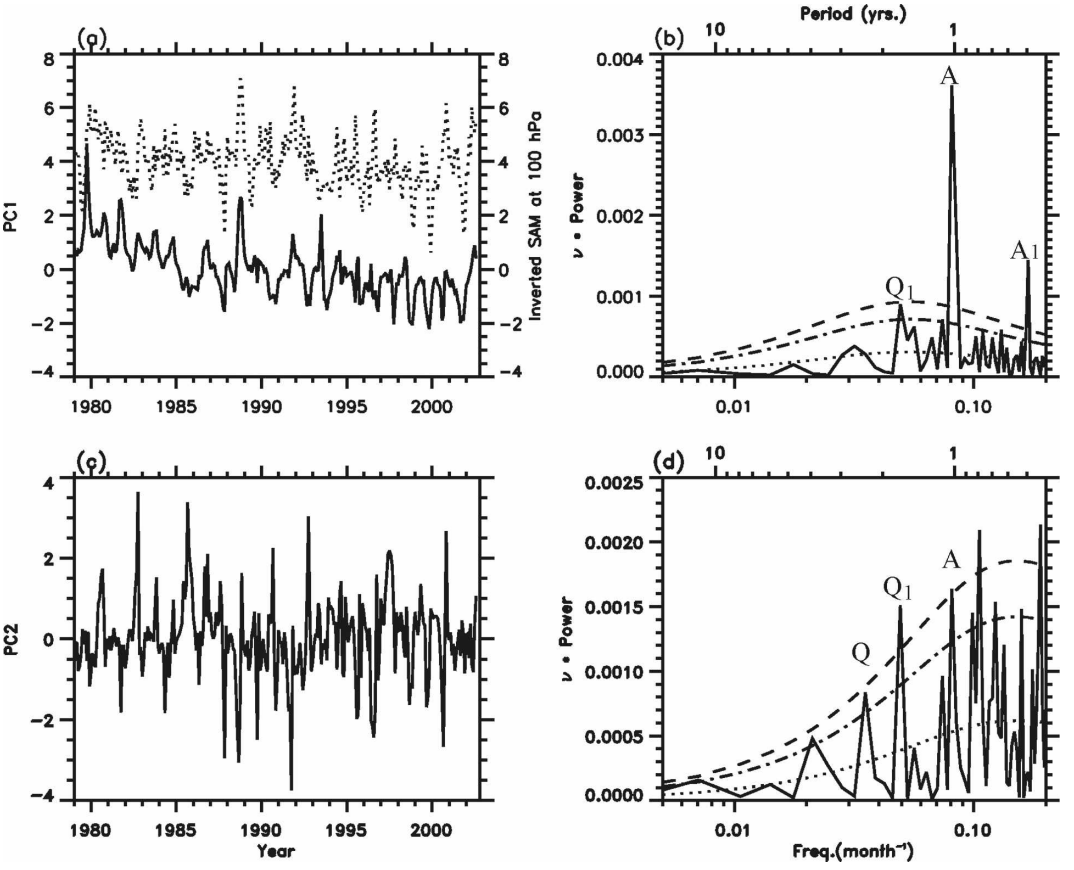

FIG. 2. (a) O_3 PC1 (solid) and inverted SAM index at 100 hPa shifted upward by 4 units (dotted) in the SH. The correlation is 0.45 (0.1% significance level). (b) Power spectral estimate of detrended PC1 (solid), red noise spectrum (dotted), and 10% and 5% significance level (dashed). (c) O_3 PC2 in the SH. (d) Power spectral estimate of detrended PC2 (solid), red noise spectrum (dotted), and 10% and 5% significance level (dashed); Q, Q_1, A, and A_1 denote the QBO, QBO-AB, residual seasonal cycle, and SAO, respectively.

around 20 (Q_1), 28 (Q), and 9 months. The time series of PC3 and PC4 are shown in Figs. 3a,c. The power spectra of the detrended PC3 and PC4 display peaks at shorter periods. Significant peaks also appear around 20 (Q_1) and 28 months (Q) for PC3, as well as a significant peak around 24 months (B) for PC4. The maxima and minima of modes 3 and 4 are not stationary, as seen by the histogram for the longitudes at which the maxima of the combined pattern for modes 3 and 4 (Fig. 3e). Hence, although these latter two modes may represent the wobbling and displacement of the polar vortex in response to planetary waves, results shown in Fig. 3e suggest that these waves are not stationary in phase, as observed in the NH case (Fig. 4e in Part I).

b. Results for Southern Hemispheric GPT

The first four modes of the NCEP2 GPT data from 10° to 90°S are shown in Fig. 4. These four modes capture over 80% of the variance. Similar to the NH, there are similarities in the structure of the first, third, and fourth modes of ozone and GPT. The first mode, capturing 29% of the total variance, is related to the SAM. The third and fourth modes capture 18.9% and 10.3% of the total variance, respectively. They represent the wavenumber-1 component in the GPT. The PC1, PC3, and PC4 time series for the layer thickness are correlated with the corresponding PCs in the SH ozone, with correlation coefficients of 0.55, 0.4, and 0.71, respectively. The statistical significance is within 1% significance level for all three cases. The spectrum of the detrended PC1 (Fig. 5b) shows peaks around 20 (Q_1) and 8 months (Q_1'). Figures 5f and 5h show the spectra of detrended PC3 and PC4. Most signals are at high frequencies.

As in the NH case, the second mode, capturing 22.4% of the total variance, is not similar to the second mode in the ozone. The second mode of GPT anomalies in the SH has a node around 55°S; that for the O_3

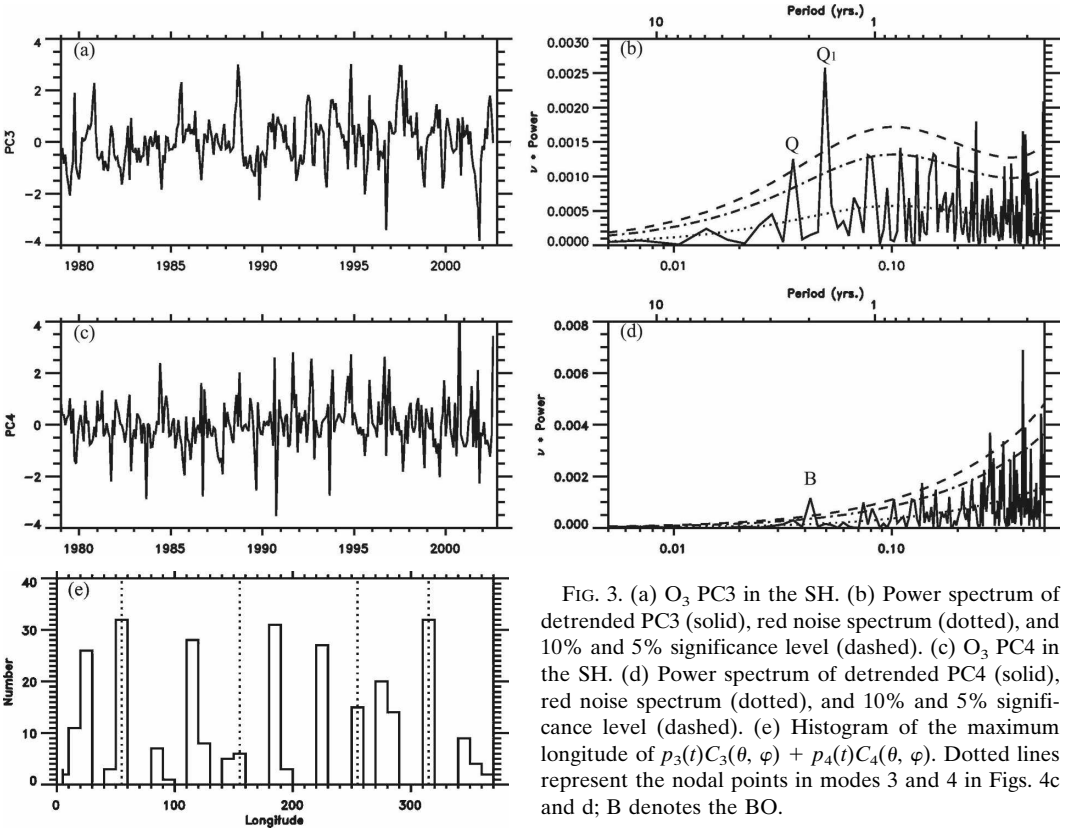

FIG. 3. (a) O_3 PC3 in the SH. (b) Power spectrum of detrended PC3 (solid), red noise spectrum (dotted), and 10% and 5% significance level (dashed). (c) O_3 PC4 in the SH. (d) Power spectrum of detrended PC4 (solid), red noise spectrum (dotted), and 10% and 5% significance level (dashed). (e) Histogram of the maximum longitude of $p_3(t)C_3(\theta, \varphi) + p_4(t)C_4(\theta, \varphi)$. Dotted lines represent the nodal points in modes 3 and 4 in Figs. 4c and d; B denotes the BO.

column has a node around 60°S. The power spectral estimate of PC2 has a peak at 8 yr, which is absent from the PC2 for column O_3. The 8-yr signal might be related to the solar cycle or low-frequency ocean oscillations. As in the NH, we conclude that the second modes of GPT and column O_3 do not match.

4. IAV and trends of column O_3 in the GEOS-CCM

a. *IAV of model column O_3*

A similar analysis is now applied to the column O_3 in the GEOS-CCM in the SH. The spatial pattern of the first mode and the PC1 time series in the SH are shown in Figs. 6a,b. The first mode in the SH, capturing 59.5% of the total variance, is also zonally symmetric and the maximum value is higher than that in the NH. The spatial pattern is similar to that in the observed O_3, but the positive and negative extremes are higher, meaning that the meridional gradient of ozone is stronger in the simulation than in the atmosphere. The correlation coefficient between the detrended PC1 of model O_3 and the detrended PC1 of the model at 30–100-hPa GPT is 0.68. The trend for the PC1 of the model O_3 in the SH is -0.1 ± 0.042 yr^{-1}, which is close to the trend for the PC1 (-0.093 ± 0.042 yr^{-1}) of the combined O_3 in the SH. For the model O_3 in the SH, the second, third, and fourth modes account for 9.9%, 9.0%, and 5.8% of the total variances. The spatial patterns for these modes are also similar to those in the SH combined O_3 data.

b. *Comparison of column O_3 trends between data and model*

The trend derived from the first mode of column O_3 in the SH (black line in Fig. 7) is largest at high latitude. It agrees well with that from the empirical mode decomposition (EMD) method (Huang et al. 1998; shown by diamonds in Fig. 7). The O_3 trend in the SH is larger than that in the NH. There is a discrepancy between the trends deduced from observations and the GEOS-CCM, but the explanation is different from that in the NH (Part I). The time series of PCs have similar trends, but in the SH the meridional gradient of ozone (represented in EOF1) is larger in the model than that in the observation. This reflects the time-dependent ozone bias discussed in Pawson et al. (2008): with low chlorine loading, the modeled ozone distribution is biased high, but at peak chlorine loading (as in the late 1990s) the

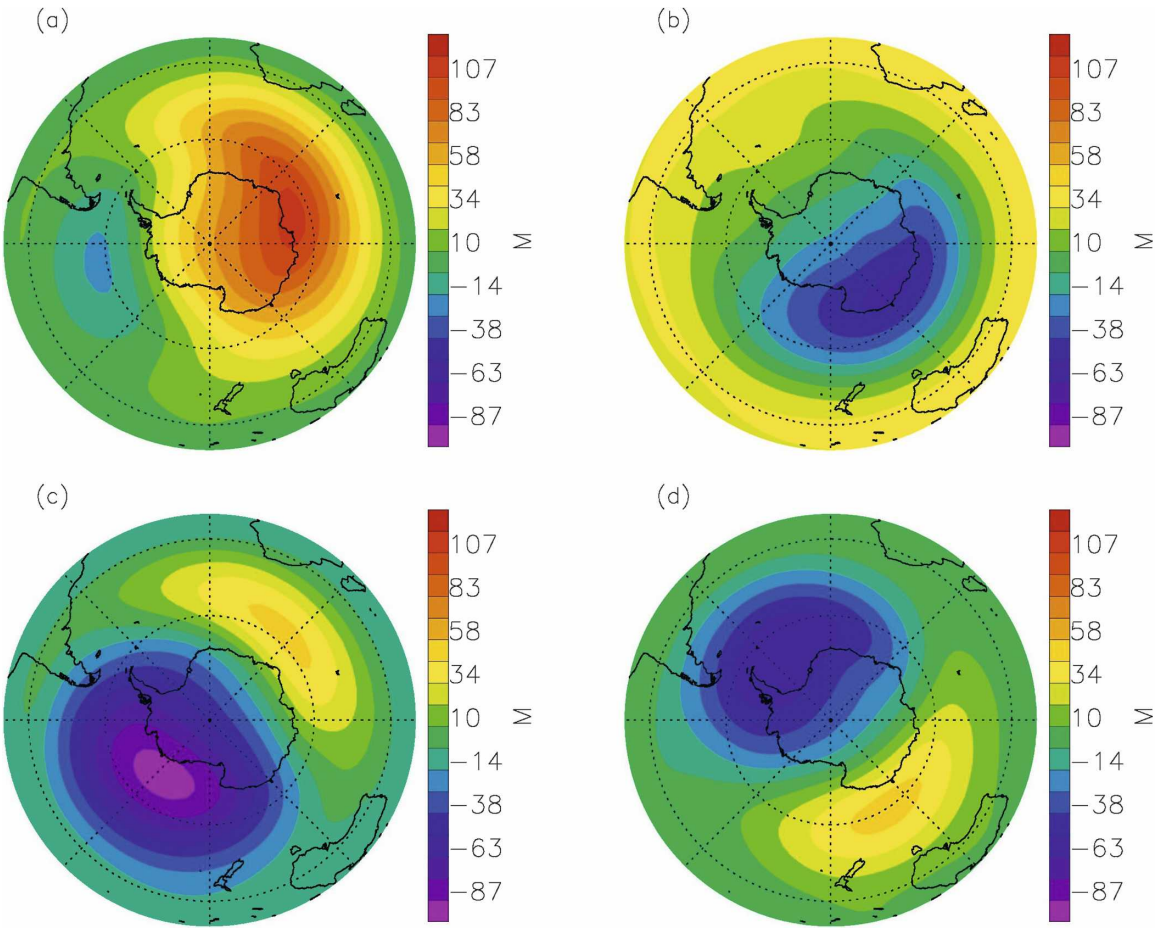

FIG. 4. The spatial patterns of the 30- to 100-hPa layer thickness anomalies regressed upon the leading PCs in the SH. Units are meters. The first four modes explain 29%, 22.4%, 18.9%, and 10.3% of the total variance, respectively.

catalytic destruction of ozone in the Antarctic spring swamps this bias, leading to closer agreement with observations, and hence to an overestimate in the trend.

5. Discussion

We discuss here how our principal findings from this work and Part I relate to other studies.

a. IAV and leading modes

We will provide a heuristic reasoning for the key result of the PCA analysis: the large fraction of IAV explained by the four leading modes. Column O_3 is an approximate conservative tracer in the stratosphere, where dynamical disturbances usually originate from the troposphere. The theorem by Charney and Drazin (1961) states that only planetary disturbances with the longest wavelengths can propagate from the lower to the upper atmosphere. Thus, the stratosphere acts as a natural low-pass filter; only the largest planetary patterns get excited.

The fundamental modes in the IAV of O_3 reported in this work appear to be robust. Results from MOD are supported by GEOS-CCM. The patterns for O_3 column are similar to those for GPT between 30 and 100 hPa, suggesting a common dynamical origin.

b. Ozone effect on temperature

Ozone is a radiatively active molecule and has direct impact on temperature, and hence GPT, in the stratosphere. To investigate the effect of ozone on temperature, the Moderate Resolution Atmospheric Transmission (MODTRAN) model (Berk et al. 1989), the Air Force Research Laboratory/Geophysics Directorate moderate spectral resolution background radiance and transmission model, is used to calculate the radiative heating rates. The MODTRAN calculations are based on a 0–3000 cm^{-1} spectral for the infrared heating rates.

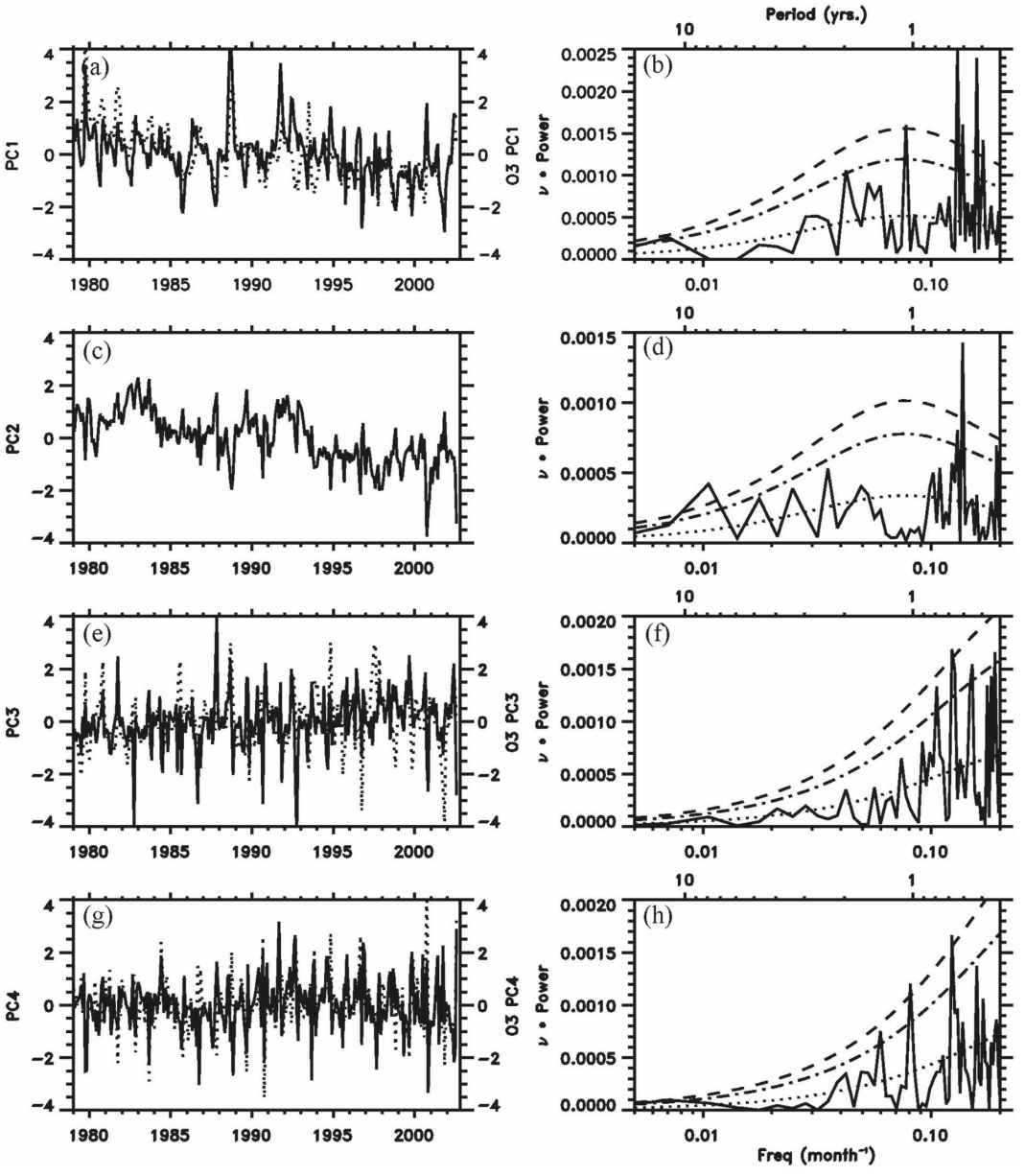

FIG. 5. (a) Layer thickness PC1 (solid) and O_3 PC1 (dotted) in the SH. The correlation is 0.55 (0.1% significance level). (b) Power spectral estimate of detrended PC1 (solid), red noise spectrum (dotted), and 10% and 5% significance level (dashed). (c), (d) As in (a), (b), but for PC2 in the SH. (e), (f) As in (a), (b), but for PC3; the correlation is 0.40. (g), (h) As in (a), (b), but for PC4; the correlation is 0.71.

For the shortwave heating rates, the calculation is based on a 5000–50 000 cm^{-1} spectral interval. We use three model atmospheres to test the results: tropical atmosphere, midlatitude summer, and subarctic winter. The effects on the net heating rates, after adding 10 Dobson Units (DU) to the stratospheric ozone, are approximately equal to the effect after decreasing the temperature by 1 K between 10 and 100 hPa. This result is consistent with that obtained by McElroy et al. (1974). From the hydrostatic balance and ideal gas law, we can obtain that a 1-K temperature change corresponds to an approximately 35-m change in GPT. Thus, at least part of the IAV of O_3 and GPT are coupled radiatively.

c. *Comparison to the tropics*

If we apply the same low-pass filter to the detrended and deseasonalized O_3 data as in Camp et al. (2003), the total variance of the first four modes is 81.8% and

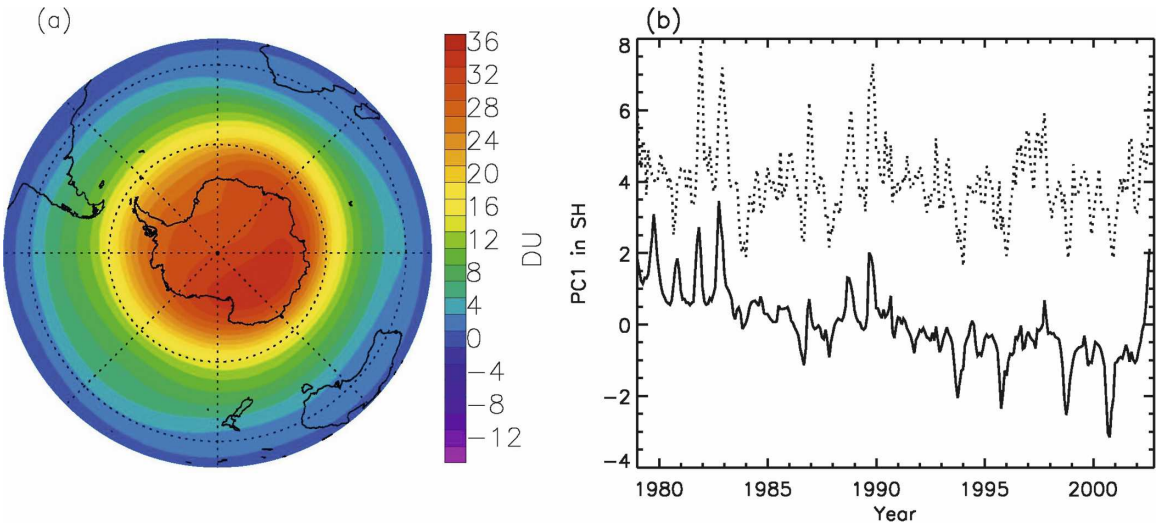

FIG. 6. (a) The spatial pattern of the model O_3 anomalies regressed upon the leading PC1 in the SH. Units are DU. The first mode explains 59.5% of the total variance. (b) PC1 of the model O_3 (solid line) and PC1 of the 30–100-hPa model GPT (dotted line) in the SH.

84.4% for the NH and SH, respectively. A low-pass filter is chosen to obtain a full signal from periods above 15 months and no signal from periods below 12.5 months. For comparison, the variances of ozone IAV of the leading modes account for 93% of the total variance in the tropics (Camp et al. 2003). For the detrended, deseasonalized, and low-pass filtered GPT, the total variances of the first four modes are 82.3% and 85.7% for the NH and SH, respectively. The variances of the leading modes are smaller than the 97% of the total variance in the tropical layer thickness (Camp et al. 2003). The reason is that there is more internal dynamics at higher latitudes (Andrews et al. 1987; Ma et al. 2004).

d. Relation to climate change

Global climate change [e.g., changes in NH annular mode (NAM) and SAM] could impact the ozone layer by modulating the transport of ozone-rich air from lower latitudes. Variations in vortex dynamics induce changes in ozone loss by heterogeneous chemistry (Austin et al. 2000; Rex et al. 2004). Because ozone is radiatively coupled to atmospheric dynamics, such a close linkage opens up possibilities for a synergistic interaction between ozone change and climate variability (Shindell et al. 1999; Thompson and Solomon 2002; Stolarski et al. 2006b).

One of the most important implications in this work is that the pattern of ozone is dominated by a few fundamental modes. By analogy with climate changes, it is possible that ozone changes, natural or anthropogenic, change the occurrence frequencies but not the structure of the fundamental modes (Corti et al. 1999). Further coupled interactive models are needed to test these ideas.

6. Conclusions

We applied PCA to the column ozone in the SH high latitude. Similar to the NH results reported in Part I in this issue, the analysis resolves the SH ozone column into zonally symmetric and asymmetric (wavenumber-1) modes (Fig. 1), with connections to the SAM, QBO, QBO–annual beat, biennial oscillation, semiannual oscillation, annual cycle, and solar cycle. The structures of these patterns appearing in the ozone record are similar

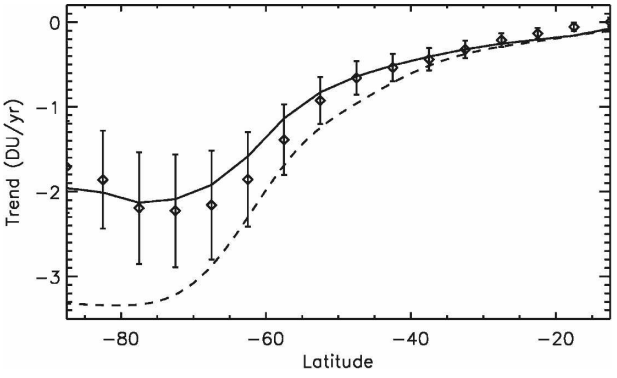

FIG. 7. Latitudinal distribution of the trend for the first mode (black) derived from column O_3 in the SH. Diamonds are results from EMD method. The dashed line is the trend from model O_3 in the SH. Units are DU per year.

TABLE A1. Years chosen to calculate the polynomial fit between the PV and O_3 data for 1989 and 1990.

		Jan	Feb	Mar	Apr	May	Jun	Jul	Aug	Sep	Oct	Nov	Dec
1989	NH	1984	1984	1984	—	—	—	—	—	1999	1999	1999	1999
	SH	—	—	1979	1979	1979	1979	1979	1979	1979	1979	—	—
1990	NH	2000	2000	2000	—	—	—	—	—	1983	1983	1983	1983
	SH	—	—	1992	1992	1992	1992	1992	1992	1992	1992	—	—

to those in the GEOS-CCM (Fig. 6) and NCEP2 GPT (Fig. 4), although there are some discrepancies between column O_3 and GPT in mode 2. The characteristics of the leading modes are summarized in Table 1. The first symmetric mode captures about 44% of the total variance in the SH, which is more than that in the NH (Part I). The cause of the difference may be less forcing by topographical and land–ocean thermal contrast in the SH than in the NH. A negative trend is seen in PC1 for SH, which reaches the minimum ~ -2DU yr^{-1} at the South Pole. In addition, the ozone trend is much larger than that of SAM. This difference may be due to the chemical loss of ozone that permanently alters the dynamics of the polar climatology of SH (Thompson and Solomon 2002). The trend and the spatial pattern for the leading mode of O_3 anomalies in the SH are well captured by the GEOS-CCM, although the trend in the NH from the model O_3 is larger than that from the combined O_3. The trend in the SH is reproduced by mode 1 in our analysis of the GEOS-CCM data. However, the model overestimates the decreasing ozone trends by ~50% at the South Pole. In the SH, the high bias in model ozone at the polar region disappears when large amounts of chlorine are activated: this re-

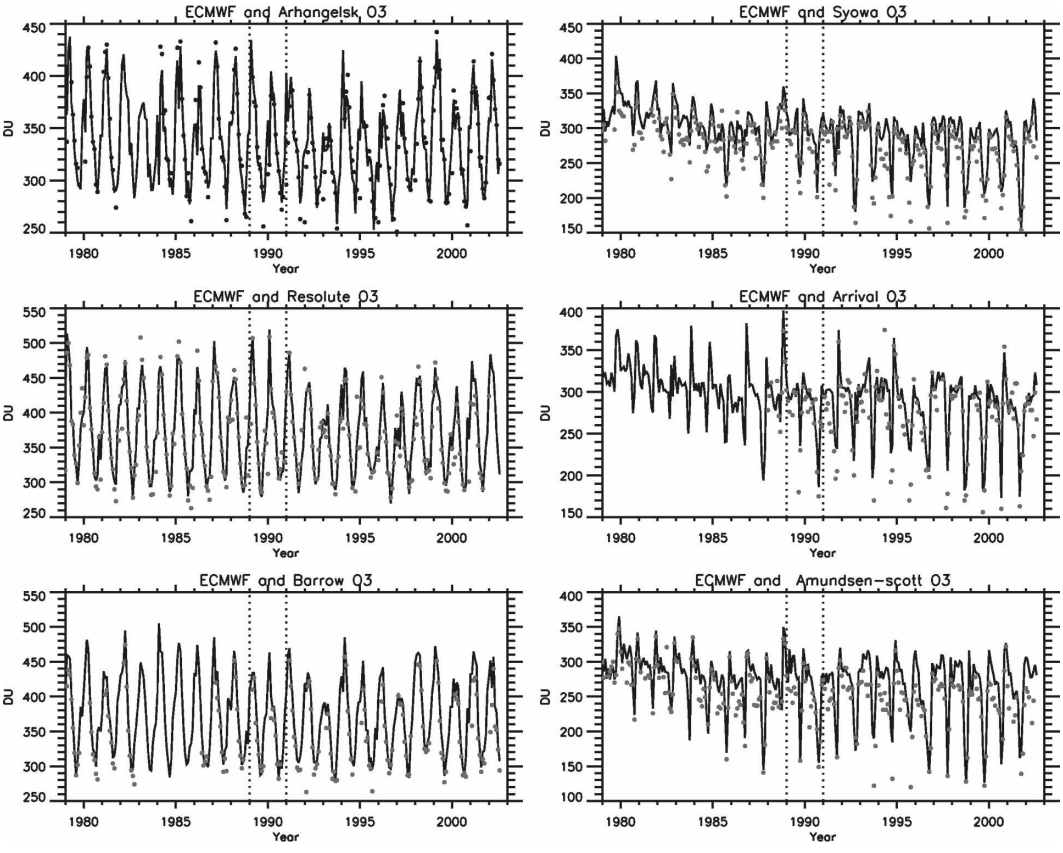

FIG. A1. Comparison of the combined MOD and ECMWF assimilated O_3 (solid) with the radiosonde ozone data (black dots) in the polar region. Arkhangelsk O_3 is at 64.58°N, 40.5°E. Resolute O_3 is at 74.72°N, 94.98°W. Barrow O_3 is at 71.32°N, 156.6°W. Syowa O_3 is at 69°S, 39.58°E. Arrival O_3 is at 77.83°S, 166.67°E. Amundsen–Scott O_3 is at 89.98°S, 24.8°W.

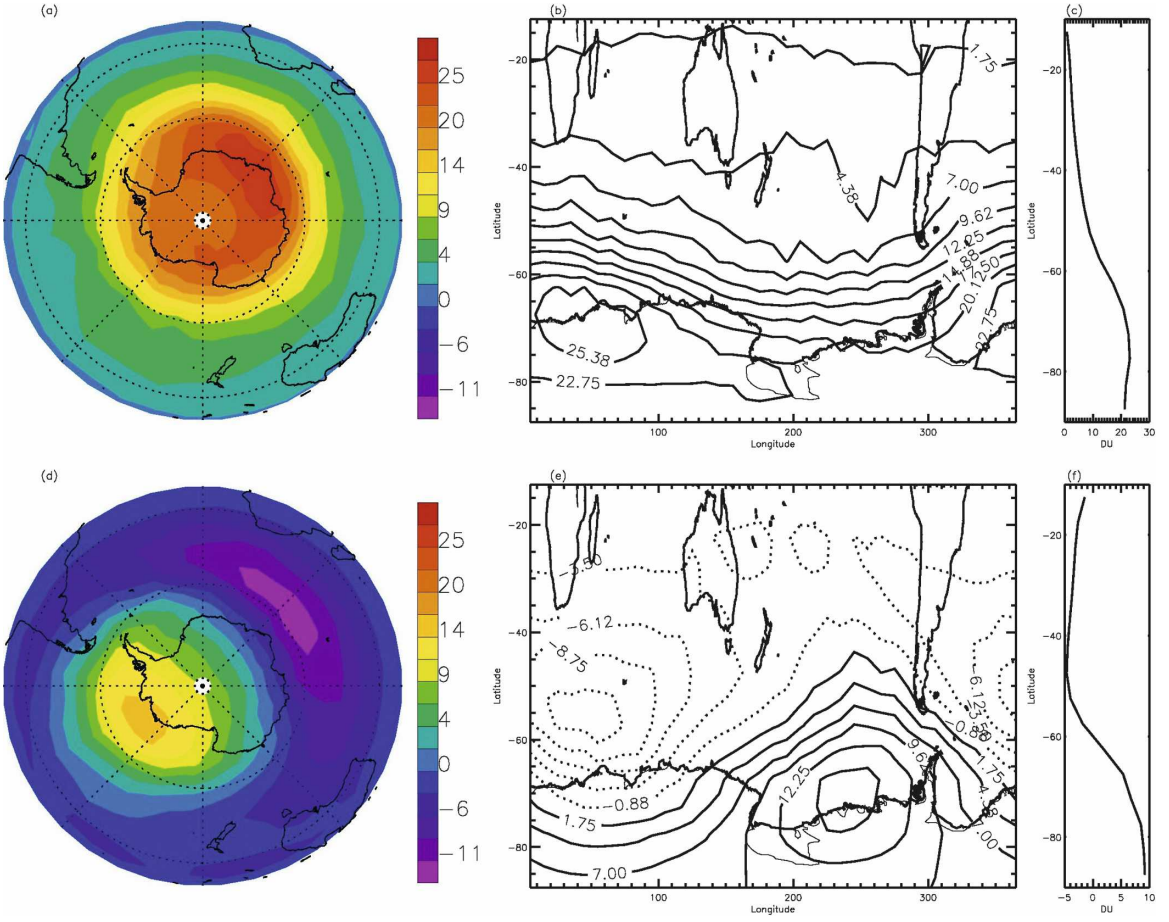

FIG. A2. The first and second modes of the combined MOD and ECMWF O_3 anomalies in the SH. (a), (d) polar projection maps; (b), (e) cylindrical projection maps; (c), (f) meridional profile of zonally averaged modes.

sults in an unrealistically large heterogeneous loss of O_3 at the pole compared to the real atmosphere.

Acknowledgments. We thank D. E. Waliser, M. Allen, D. Feldman, A. Ingersoll, J. Perkins, J. Weibel, M. Gerstell, and two anonymous reviewers for useful inputs and helpful comments. Special thanks are due to R. Stolarski for his contribution to the ozone simulations, K. Jeev for deducing the missing O_3 data using potential vorticity, L. M. Li for critical reading and editing of the manuscript, and R. Salawitch for improving presentation of results on O_3 trends. NASA provided computational resources for running the GEOS-CCM through their high-performance computing initiative (the model was run on the "Columbia" computer at NASA Ames Research Center). This research was supported in part by NASA Grants NNG04GD76G and NNG04GN02G to the California Institute of Technology. S. Pawson and E. Nielsen were supported by NASA's Modeling and Analysis Program. V. Limpasuvan was supported by NSF Grants ATM-0213248 and ATM-0521002.

APPENDIX

Validation and Figures of Ozone Data

The appendix provides information on the validation of the O_3 data, cylindrical projections, zonal mean, and *t* statistics of leading modes in the SH.

a. Validation of O_3 data

The ECMWF O_3 data are assimilated from January 1979 to December 1988 and from January 1991 to August 2002. Retrievals from total ozone mapping spectrometer (TOMS) and solar backscattered UV (SBUV) instruments on various satellites are directly assimilated. During 1989 and 1990 when the ECMWF assimilated O_3 was not available, ECMWF potential vorticity was used as a proxy for O_3 in the polar night regions. A simple mapping method is used (Manney et al. 1999). First, we choose similar winters as those in 1989 and 1990 by the annular mode indices. The details are listed in Table A1. The data for PV and O_3 (originally on pres-

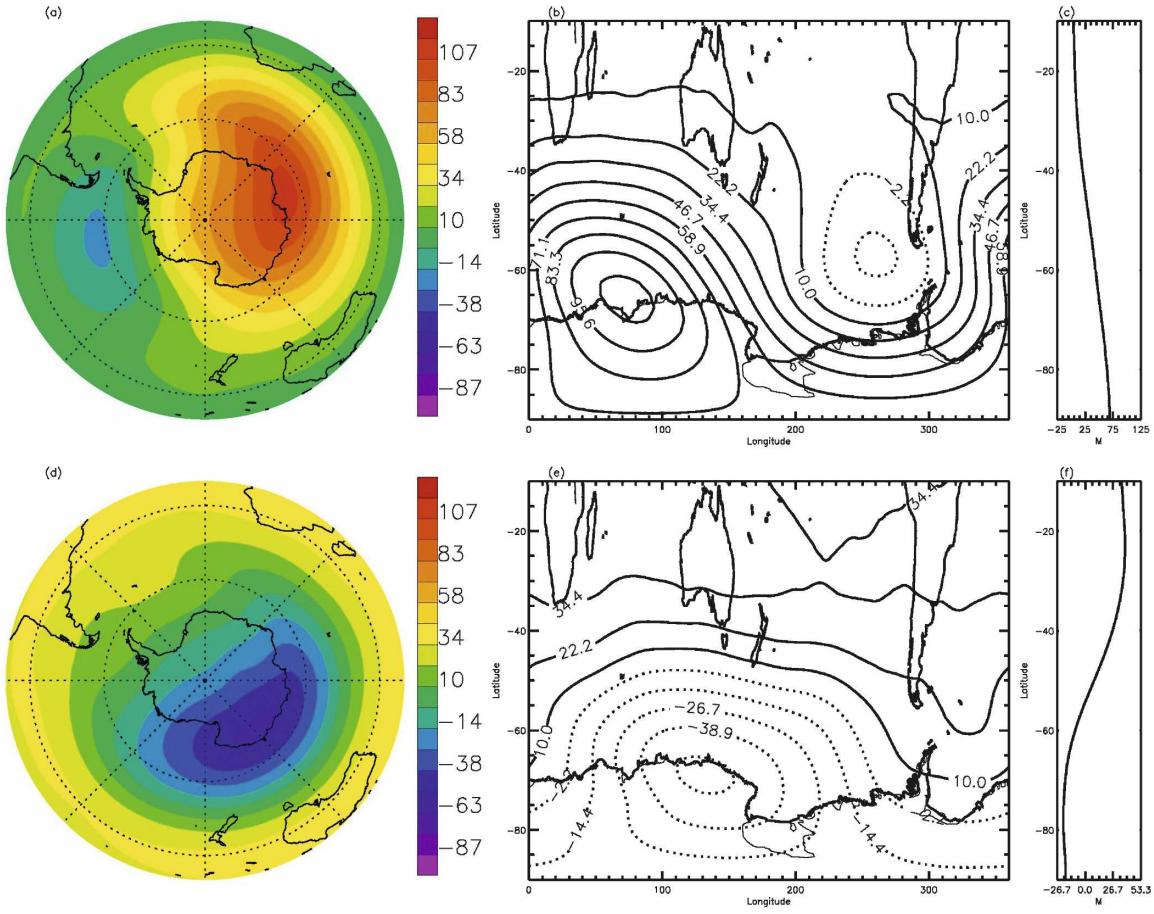

FIG. A3. The first and second modes of the 30 hPa to 100 hPa layer thickness anomalies in the SH. (a), (d) polar projection maps; (b), (e) cylindrical projection maps; (c), (f) meridional profile of zonally averaged modes.

sure surfaces) are interpolated to isentropic surfaces using a linear interpolation scheme described by Held and Schneider (1999). Then the relation between PV and O_3 is fitted to a fourth-order polynomial. Ozone values in 1989 and 1990 are calculated from PV using this polynomial fit. Finally, we interpolate the O_3 data from the isentropic surfaces back to the pressure surfaces. Ozone abundances in the troposphere are set to climatological values. We compare the ECMWF data assimilated with the MOD at different latitudes. It agrees well with the MOD. In the polar region, the radiosonde O_3 data are compared with the combined MOD and ECMWF assimilated O_3 data in Fig. A1. The combined O_3 data agree well with the radiosonde data, although the ozone hole is not deep enough at the South Pole in October.

b. *Cylindrical projections, zonal mean, and t statistics of leading modes*

The polar projection, cylindrical projection, and zonal mean of the leading two modes for the SH combined MOD and ECMWF O_3 anomalies are shown in Fig. A2. Similar results for the 30- to 100-hPa geopotential height layer thickness anomalies in the SH are shown in Fig. A3. The first mode of O_3 anomalies in the SH is positive. The second mode of O_3 anomalies in the SH has a node at approximately 60°S. The first mode of GPT anomalies is positive in the polar region and negative in the subtropical region. The second mode of GPT anomalies in the SH has a node around 55°S. The associated *t* statistics for the regression coefficients of O_3 and GPT anomalies in the SH suggest that the results are statistically significant in most areas.

REFERENCES

Andrews, D. G., J. R. Holton, and C. B. Leovy, 1987: *Middle Atmosphere Dynamics*. Academic Press, 489 pp.

Austin, J., J. R. Knight, and N. Butchart, 2000: Three-dimensional chemical model simulations of the ozone layer: 1979–2015. *Quart. J. Roy. Meteor. Soc.,* **126,** 1533–1556.

Berk, A., L. S. Bernstein, and D. C. Robertson, 1989: MODTRAN:

A moderate resolution model for LOWTRAN 7. Air Force Geophysics Laboratory Tech. Rep. 89-0122, 38 pp.

Camp, C. D., M. S. Roulston, and Y. L. Yung, 2003: Temporal and spatial patterns of the interannual variability of total ozone in the tropics. *J. Geophys. Res.,* **108,** 4643, doi:10.1029/2001JD001504.

Charney, J. G., and P. G. Drazin, 1961: Propagation of planetary-scale disturbances from the lower into the upper atmosphere. *J. Geophys. Res.,* **66,** 83–109.

Coffey, M. T., 1996: Observations of the impact of volcanic activity on stratospheric chemistry. *J. Geophys. Res.,* **101,** 6767–6780.

Corti, S., F. Molteni, and T. N. Palmer, 1999: Signature of recent climate change in frequencies of natural atmospheric circulation regimes. *Nature,* **398,** 799–802.

Da Silva, A., and Coauthors, 2005: Documentation and validation of the Goddard Earth Observation System (GEOS) data assimilation system, version 4. Nasa Tech. Rep. TM-2005-104606, Vol. 26, 166 pp.

Dethof, A., and E. V. Holm, 2004: Ozone assimilation in the ERA-40 reanalysis project. *Quart. J. Roy. Meteor. Soc.,* **130,** 2851–2872.

Fusco, A. C., and M. L. Salby, 1999: Interannual variations of total ozone and their relationship to variations of planetary wave activity. *J. Climate,* **12,** 1619–1629.

Gray, L. J., and J. A. Pyle, 1986: The semiannual oscillation and equatorial tracer distributions. *Quart. J. Roy. Meteor. Soc.,* **112,** 387–407.

Held, I. M., and T. Schneider, 1999: The surface branch of the zonally averaged mass transport circulation in the troposphere. *J. Atmos. Sci.,* **56,** 1688–1697.

Hood, L. L., and B. E. Soukharev, 2003: Quasi-decadal variability of the tropical lower stratosphere: The role of extratropical wave forcing. *J. Atmos. Sci.,* **60,** 2389–2403.

Huang, N. E., and Coauthors, 1998: The empirical mode decomposition and Hilbert spectrum for nonlinear and non-stationary time series analysis. *Proc. Roy. Soc. London,* **454A,** 903–995.

Jiang, X., D. B. A. Jones, R. Shia, D. E. Waliser, and Y. L. Yung, 2005: Spatial patterns and mechanisms of the quasi-biennial oscillation—Annual beat of ozone. *J. Geophys. Res.,* **110,** D23308, doi:10.1029/2005JD006055.

——, S. Pawson, C. D. Camp, J. E. Nielsen, R.-L. Shia, T. Liao, V. Limpasuvan, and Y. L. Yung, 2008: Interannual variability and trends of extratropical ozone. Part I: Northern Hemisphere. *J. Atmos. Sci.,* **65,** 3013–3029.

Li, F., J. Austin, and J. Wilson, 2008: The strength of the Brewer–Dobson circulation in a changing climate: Coupled chemistry–climate model simulations. *J. Climate,* **21,** 40–57.

Kalnay, E., and Coauthors, 1996: The NCEP/NCAR 40-Year Reanalysis Project. *Bull. Amer. Meteor. Soc.,* **77,** 437–471.

Kistler, R., and Coauthors, 2001: The NCEP–NCAR 50-Year Reanalysis: Monthly means CD-ROM and documentation. *Bull. Amer. Meteor. Soc.,* **82,** 247–267.

Limpasuvan, V., and D. L. Hartmann, 1999: Eddies and the annular modes of climate variability. *Geophys. Res. Lett.,* **26,** 3133–3136.

Ma, J., D. W. Waugh, A. R. Douglass, S. R. Kawa, P. A. Newman, S. Pawson, R. Stolarski, and S. J. Lin, 2004: Interannual variability of stratospheric trace gases: The role of extratropical wave driving. *Quart. J. Roy. Meteor. Soc.,* **130,** 2459–2474.

Manney, G. L., H. A. Michelsen, M. L. Santee, M. R. Gunson, F. W. Irion, A. E. Roche, and N. J. Livesey, 1999: Polar vortex dynamics during spring and fall diagnosed using trace gas observations from the Atmospheric Trace Molecule Spectroscopy instrument. *J. Geophys. Res.,* **104,** 18 841–18 866.

McElroy, M. B., S. C. Wofsy, J. E. Penner, and J. C. McConnell, 1974: Atmospheric ozone: Possible impact of stratospheric aviation. *J. Atmos. Sci.,* **31,** 287–303.

McPeters, R., and Coauthors, 1996: Nimbus-7 Total Ozone Mapping Spectrometer (TOMS) data products user's guide. NASA Reference Publication 1384, 67 pp.

Pawson, S., R. S. Stolarski, A. R. Douglass, P. A. Newman, J. E. Nielsen, S. M. Frith, and M. L. Gupta, 2008: Goddard Earth Observing System chemistry–climate model simulations of stratospheric ozone–temperature coupling between 1950 and 2005. *J. Geophys. Res.,* **113,** D12103, doi:10.1029/2007JD009511.

Pollack, J. B., O. B. Toon, E. F. Danielsen, D. J. Hofmann, and J. M. Rosen, 1983: The El Chichón volcanic cloud: An introduction. *Geophys. Res. Lett.,* **10,** 989–992.

Preisendorfer, R. W., 1988: *Principal Component Analysis in Meteorology and Oceanography*. Elsevier, 425 pp.

Randel, W. J., F. Wu, and R. Stolarski, 2002: Changes in column ozone correlated with the stratospheric EP flux. *J. Meteor. Soc. Japan,* **80,** 849–862.

Rex, M., R. J. Salawitch, P. von der Gathen, N. R. P. Harris, M. P. Chipperfield, and B. Naujokat, 2004: Arctic ozone loss and climate change. *Geophys. Res. Lett.,* **31,** L04116, doi:10.1029/2003GL018844.

Shindell, D. T., R. L. Miller, G. A. Schmidt, and L. Pandolfo, 1999: Simulation of recent northern winter climate trends by greenhouse-gas forcing. *Nature,* **399,** 452–455.

——, G. Faluvegil, N. Unger, E. Aguilar, G. A. Schmidt, D. M. Koch, S. E. Bauer, and R. L. Miller, 2006: Simulations of preindustrial, present-day, and 2100 conditions in the NASA GISS composition and climate model G-PUCCINI. *Atmos. Chem. Phys.,* **6,** 4427–4459.

Simmons, A. J., A. Untch, C. Jakob, P. Kallberg, and P. Unden, 1999: Stratospheric water vapour and tropical tropopause temperatures in ECMWF analyses and multi-year simulations. *Quart. J. Roy. Meteor. Soc.,* **125,** 353–386.

Stolarski, R. S., A. R. Douglass, M. Gupta, P. A. Newman, S. Pawson, M. R. Schoeberl, and J. E. Nielsen, 2006a: An ozone increase in the Antarctic summer stratosphere: A dynamical response to the ozone hole. *Geophys. Res. Lett.*, **33,** L21805, doi:10.1029/2006GL026820.

——, ——, S. E. Steenrod, and S. Pawson, 2006b: Trends in stratospheric ozone: Lessons learned from a 3D chemical transport model. *J. Atmos. Sci.,* **63,** 1028–1041.

Thompson, D. W. J., and J. M. Wallace, 2000: Annular modes in the extratropical circulation. Part I: Month-to-month variability. *J. Climate,* **13,** 1000–1016.

——, and S. Solomon, 2002: Interpretation of recent Southern Hemisphere climate change. *Science,* **296,** 895–899.

Trepte, C. R., R. E. Veiga, and M. P. McCormick, 1993: The poleward dispersal of Mount Pinatubo volcanic aerosol. *J. Geophys. Res.,* **98,** 18 563–18 574.

Tung, K.-K., and H. Yang, 1994a: Global QBO in circulation and ozone. I. Reexamination of observational evidence. *J. Atmos. Sci.,* **51,** 2699–2707.

——, and ——, 1994b: Global QBO in circulation and ozone II. A simple mechanistic model. *J. Atmos. Sci.,* **51,** 2708–2721.

Uppala, S. M., and Coauthors, 2005: The ERA-40 re-analysis. *Quart. J. Roy. Meteor. Soc.,* **131,** 2961–3012.

Zerefos, C. S., K. Tourpali, and A. F. Bais, 1994: Further studies on possible volcanic signal to the ozone layer. *J. Geophys. Res.,* **99,** 25 741–25 746.